Geometrical determinant of nonlinear synaptic integration in human cortical pyramidal neurons

Jaeyoung Yoon[1,2,*], *(TBD)*[†]

[1] McGovern Institute for Brain Research, Massachusetts Institute of Technology, Cambridge, MA 02139, USA.
[2] Present address: F.M. Kirby Neurobiology Center, Boston Children's Hospital, Boston, MA 02115, USA.
[*] Correspondence: jy.yoon@tch.harvard.edu
[†] *Full author list to be determined*

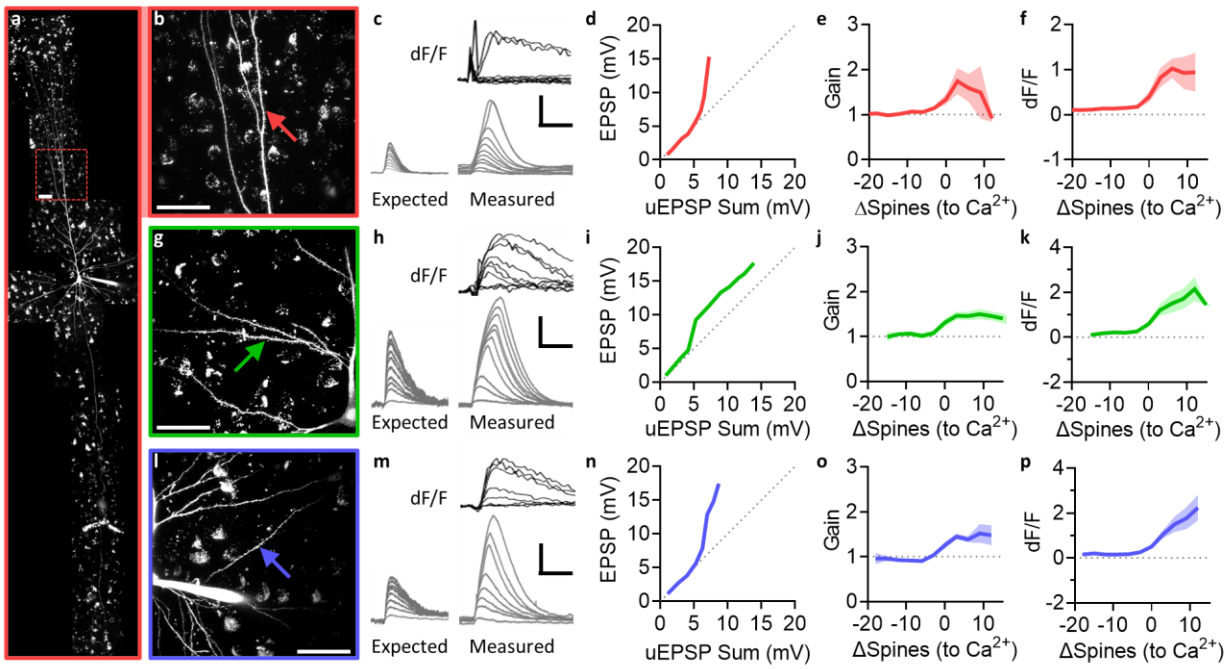

Figure 1. Synaptic integration at human neocortical layer 2/3 pyramidal neurons (L2/3 PN). **(a)** Representative example of an L2/3 PN. Scale bar, 50 um. **(b)** Same cell as in panel **a**, at the apical tuft. Arrow indicates the center of synaptic spines, which typically spanned approximately 30-40 um along the length of the branch, that were activated by 2-photon glutamate uncaging (2PGU). **(c)** Representative examples of expected EPSP (left), calculated from the arithmetic sum of unitary EPSP (uEPSP) recorded from each spine, and measured EPSP (right, bottom) recorded by quasi-simultaneous activation of spines shown in panel **b**, along with associated dF/F traces (right, top) obtained by intracellular calcium imaging. Scale bars, 50 ms, 5 mV, 1.0 dF/F. **(d)** Representative example of measured EPSP, plotted against the arithmetic sum of uEPSPs, from the activation of the same spines as shown in panels **b-c**. **(e)** Grouped average from all apical tuft dendrites (n = 24). Gain is defined by the ratio of measured vs. expected EPSP, or the measured EPSP divided by the sum of corresponding uEPSPs. The number of activated spines are aligned to the threshold at which Ca^{2+} signal was first observed. **(f)** Grouped average of dF/F, associated with data shown in panel **e**. **(g-k)** Similar to panels **b-f**, but from oblique dendrites (n = 16) branching from the apical trunk. **(l-p)** Similar to panels **b-f** or **g-k**, but from basal dendrites (n = 20) branching from the soma.

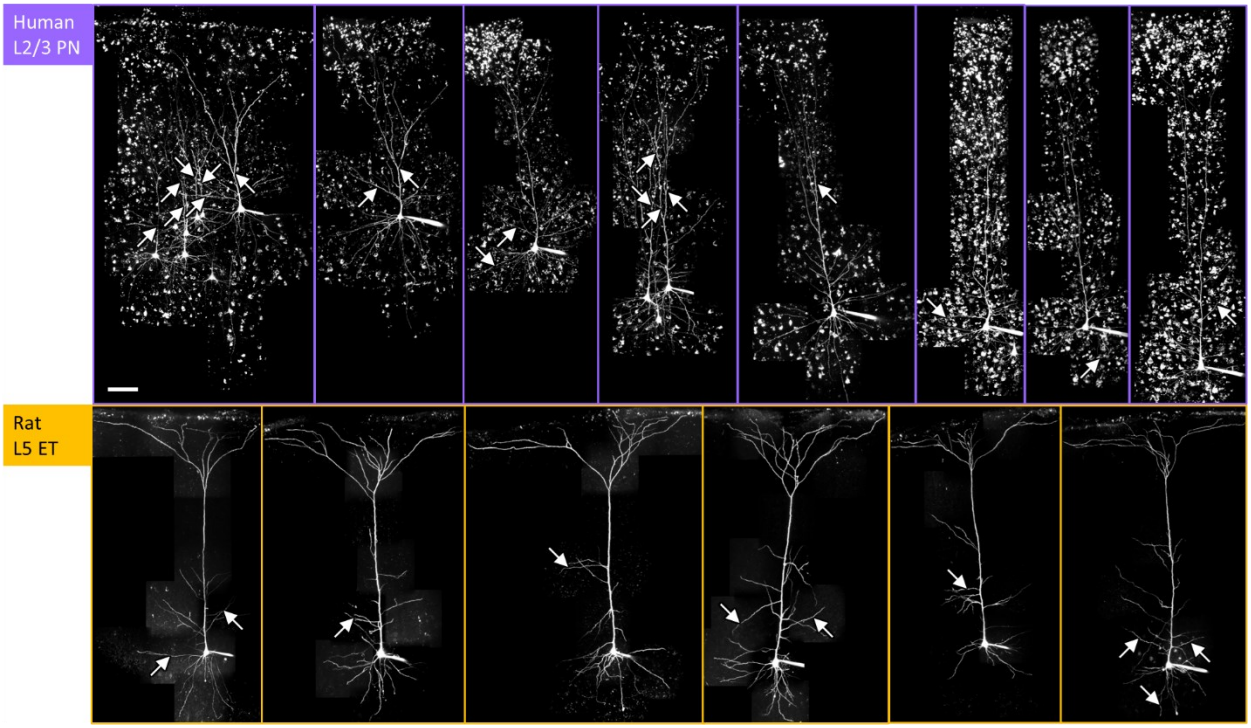

Figure 2. Representative examples showing the location of synaptic spines activated by 2PGU. For simplicity, arrows indicate the center of the spine clusters. Top, human L2/3 PN; the high background noise in human cortical images is due to lipofuscin aggregates on the somata of neurons. Bottom, rat L5 extratelencephalic (ET) cells. Scale bar, 100 um.

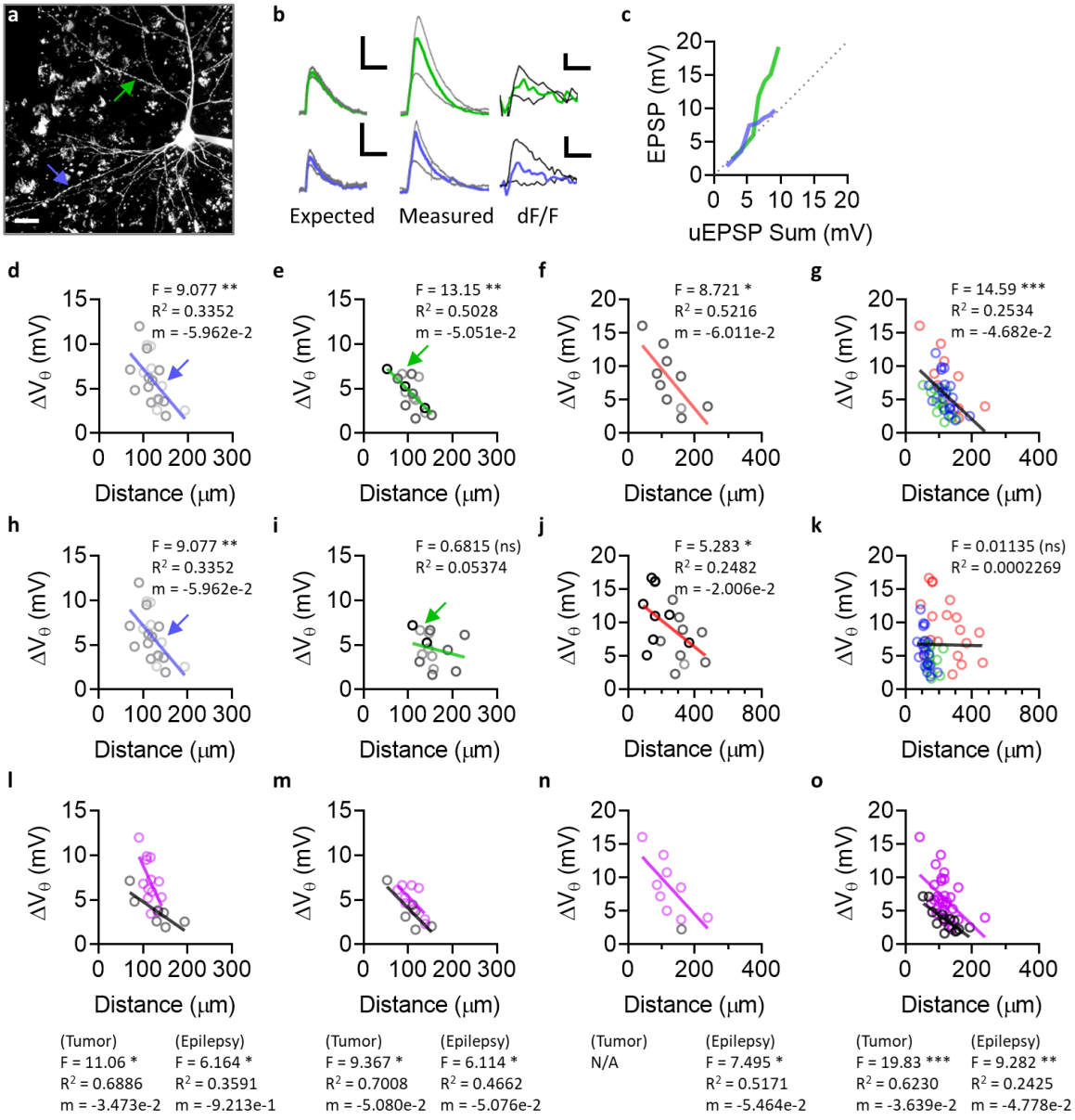

Figure 3. Somatic threshold potential at supralinearity is determined by the distance between the synaptic spines and the primary structure of human cortical neurons. **(a)** Representative example of a human L2/3 PN. Two different uncaging locations, one on a basal dendrite (blue) and another on an oblique dendrite (green), are indicated by arrows. Scale bar, 50 um. **(b)** Representative traces of expected and measured EPSP, along with associated dF/F, from the branches shown in panel **a**. Scale bars, 50 ms, 5 mV, 0.5 (bottom) or 0.1 (top) dF/F. **(c)** Measured EPSP vs. expected EPSP from uEPSP sum, from the same branches shown in panels **a-b**. **(d-g)** Somatic nonlinearity threshold potential (ΔV_θ), plotted against the curvilinear distance to primary structure. ΔV_θ was defined by the somatic uEPSP sum at local nonlinearity threshold indicated by local Ca^{2+} signal.

The primary structure was defined as the soma and its immediate extension along the apical trunk up to any branch point. For ΔV_θ, expected EPSP from uEPSP sum was used instead of the actual measured EPSP to determine the accurate threshold irrespective of the nonlinear gain. **(d)** ΔV_θ at basal dendrites vs. distance to primary structure (soma). Different shades of symbols indicate increasing branch order (1st to 4th, darker to lighter, throughout panels **d-f**). **(e)** ΔV_θ at oblique dendrites vs. distance to primary structure (branch point at the apical trunk). **(f)** ΔV_θ at apical tuft dendrites vs. distance to primary structure (branch point at the apical trunk, i.e. nexus). **(g)** Data shown in panels **d-f**, overlaid for comparison. **(h-k)** similar to panels **d-g**, but plotted against distance to soma instead of primary structure; note that by definition of primary structure, panel **h** is identical to panel **d**. **(l-o)** Same data as in panels **d-g**, but grouped separately by tumor (black) or epilepsy (purple).

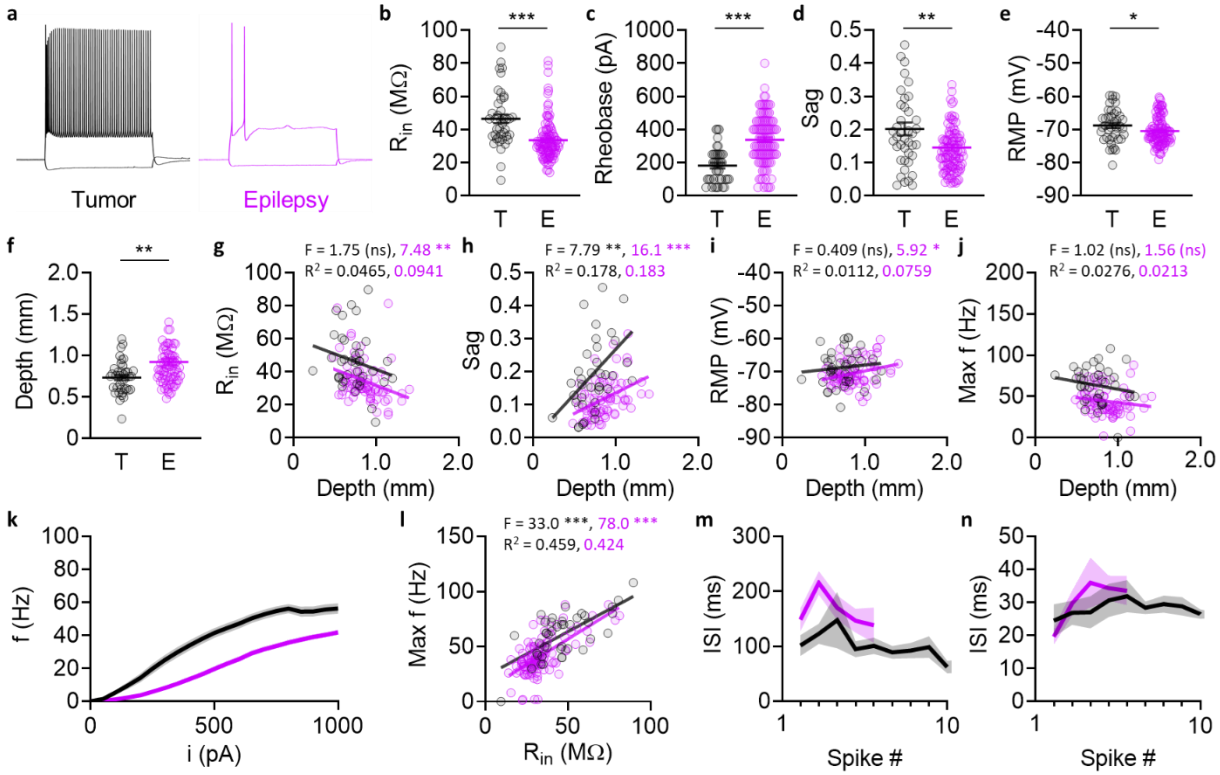

Figure 4. Intrinsic membrane properties of L2/3 PN, from tumor (black) or epilepsy (purple). For more detailed patient information, see **Table 1**. Note that tissue from both tumor and epilepsy patients originated from areas determined to be nonpathological, but removed as part of the surgical procedure. **(a)** Representative traces of membrane potential responses to somatic step current injection (-250 pA, +1000 pA). The example to the right was taken from the same cell as in **Fig. 1a**. **(b)** Input resistance (R_{in}). See methods for R_{in} calculation. **(c)** Rheobase, with current step resolution of 50 pA. **(d)** Sag ratio. See methods for the definition of sag ratio. **(e)** Resting membrane potential (RMP). **(f)** Sampling bias in the cortical depths of recorded L2/3 PNs included in the current study. Cortical depth of a recorded cell was defined as the linear distance between the pial surface and the center of the soma, extrapolated from the line connecting the soma and the nexus. **(g-j)** Intrinsic membrane properties, plotted against cortical depth. **(g)** R_{in}. **(h)** Sag ratio. **(i)** RMP. **(j)** Peak firing rate. **(k)** Firing frequency in response to somatic current injection (f-i curve). **(l)** Peak firing rate, plotted against R_{in}. **(m)** Inter-spike interval (ISI) at rheobase. **(n)** ISI at 2*rheobase.

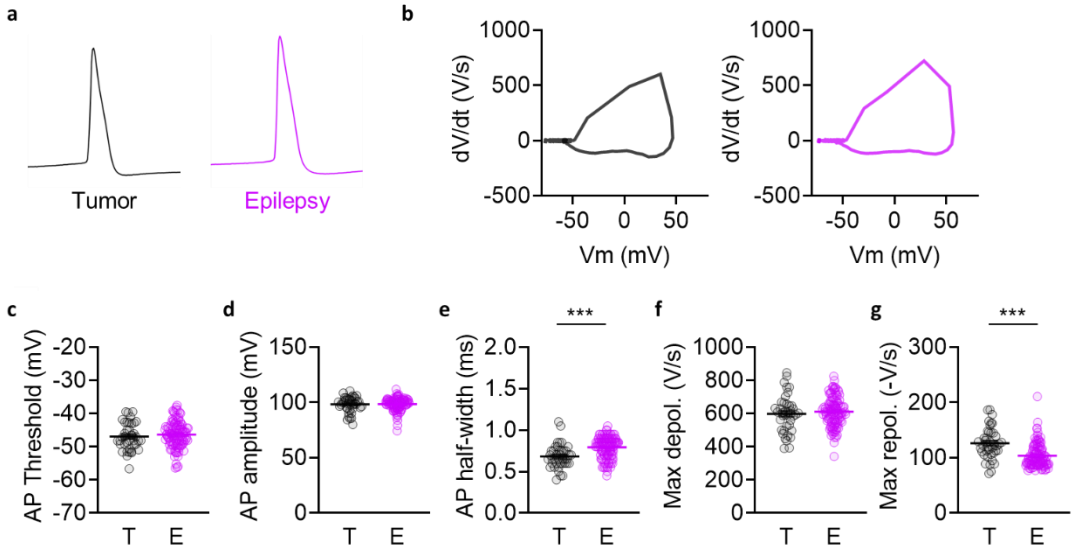

Figure 5. Single action potential (AP) kinetics of L2/3 PN, from tumor (black) or epilepsy (purple). **(a)** Representative traces. For each cell, the first action potential generated at rheobase was taken for analysis. The example to the right was taken from the same cell as in **Fig. 3a**. **(b)** Example AP waveforms presented as dV/dt plots, calculated from the same traces as in panel **a**. **(c)** AP threshold. AP threshold was defined as the V_m at which dV/dt crossed 10 (V/s). **(d)** AP amplitude (RMP to AP peak). **(e)** AP half-width. **(f)** Maximum rate of depolarization. **(g)** Maximum rate of repolarization.

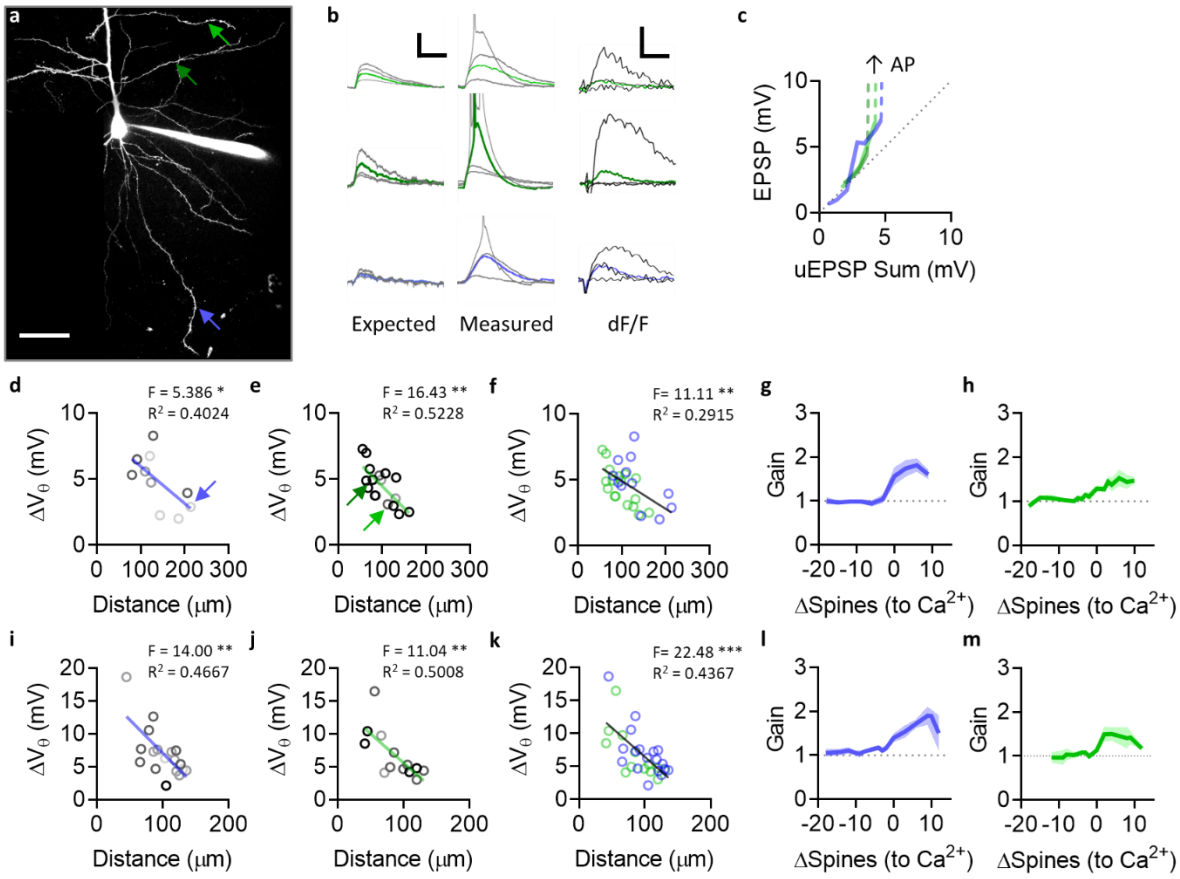

Figure 6. Somatic threshold potential at supralinearity is linearly correlated to synapse distance from primary structure in rodents as well as in humans, for both supragranular and infragranular rodent cortical pyramidal neurons. **(a)** Representative example of a rat L5 ET PN, from the temporal association area (TeA). Three different uncaging locations, one on a basal dendrite and two on separate oblique dendrites, are indicated by arrows. Scale bar, 50 um. **(b)** Representative traces from the uncaging locations shown in panel a. Scale bars, 50 ms, 5 mV, 0.5 dF/F. **(c)** Measured EPSP vs. expected EPSP from uEPSP sum, from the branches shown in panels **a-b**. **(d-f)** ΔV_θ vs. distance to primary structure, in rat L5 ET. **(d)** Basal dendrites. **(e)** Oblique dendrites. **(f)** Data shown in panels **d-e**, overlaid for comparison. **(g)** Synaptic gain, at basal dendrites shown in panel **d**. **(h)** Synaptic gain, at oblique dendrites shown in panel **e**. **(i-m)** Similar to panels **d-h**, but from rat L2/3 PNs instead of L5 ET. **(i)** Basal dendrites. **(j)** Oblique dendrites. **(k)** Data shown in panels **i-j**, overlaid for comparison. **(l)** Synaptic gain, at basal dendrites shown in panel **i**. **(m)** Synaptic gain, at oblique dendrites shown in panel **j**.

101

ID	Age	Sex	Area	Hemi.	Medications (AED)*	Diagnosis	n (cells/humans)
211102	55	M	ATL	R	(N/A)	Tumor	10
211105	32	M	TL	L	Cb, Le, O, T	Epilepsy	2
211110	71	F	TL	R	(N/A)	Tumor	13
211118	46	M	FL	L	Ce, O, Ph	Epilepsy	7
211206	71	M	TL	R	(N/A)	Epilepsy	13
220307	33	M	FL	R	B, Lc, Lo	Epilepsy	12
220317	23	F	ATL	R	Cn, G, Lm, Le, Lo, T, Z	Epilepsy	43†
220331	24	M	ATL	R	Lc, Le, O, T	Epilepsy	1
220705	18	F	TL	R	Cb, G, Lm, Le, O, T	Epilepsy	6
220815	57	F	TL	R	(N/A)	Tumor	9
220816	24	M	TL	R	E, G, Lm, Le, O, Pe	Epilepsy	16
220908	30	M	TL	L	Lm, Le	Epilepsy	1
230131	72	F	TL	R	(N/A)	Tumor	4
230216	31	M	TL	R	(N/A)	Epilepsy	7
230315	71	M	TL	R	(N/A)	Tumor	7
						(Tumor)	43/5
						(Epilepsy)	108/10
						(Total)	151/15

* Abbreviations:
B, brivaracetam; Ce, cenobamate; Cb, clobazam; Cn, clonazepam; E, eslicarbazepine; G, gabapentin; Lc, lacosamide; Lm, lamotrigine; Le, levetiracetam; Lo, lorazepam; O, oxcarbazepine; Pe, perampanel; Ph, phenytoin; T, topiramate; Z, zonisamide; N/A, not available (not applicable or unknown).

† Recorded up to 120 h post-resection (typically 24 to 48 h)

102 **Table 1.** Patient information.

103

Methods

Brain slice preparation

For human brain slices, resected tissue was immediately placed in an ice-cold solution at the operating theater. The cutting solution used for transport and slicing contained (in mM): 165 sucrose, 20 HEPES, 25 $NaHCO_3$, 2.5 KCl, 1.25 NaH_2PO_4, 20 D-glucose, 5 Na-ascorbate, 3 Na-pyruvate, 0.5 $CaCl_2$, 7 $MgCl_2$, pH adjusted to 7.3, 300-310 mOsm. All compounds were obtained from Sigma Aldrich unless otherwise specified. The tissue container was kept in a thermally isolated transportation box filled with ice packs and transported from the operating room at Massachusetts General Hospital (MGH) or Brigham and Women's Hospital (BWH) to the laboratory at Massachusetts Institute of Technology (MIT) within 25 minutes. The tissue block was then placed orthogonal to the pia to preserve cortical layers and white matter in proper orientation. Slices of 300 µm thickness were prepared with a vibratome (VT1200S, Leica), and maintained at 36 °C for at least 1 hour in the recovery solution containing (in mM): 90 NaCl, 20 HEPES, 25 $NaHCO_3$, 2.5 KCl, 1.25 NaH_2PO_4, 20 D-glucose, 5 Na-ascorbate, 3 Na-pyruvate, 1 $CaCl_2$, 4 $MgCl_2$, pH adjusted to 7.3, 300-310 mOsm. All solutions were continuously aerated with 95% O2 / 5% CO2 (pH 7.4) throughout the course of experiments, including transport and slicing. Experiments were performed typically within a period of 24 or 48 hours following resection, with exception (see Table 1). For rodent brain slices, animals were anesthetized with isoflurane inhalation prior to decapitation, and the cutting solution contained (in mM): 75 sucrose, 75 NaCl, 25 $NaHCO_3$, 2.5 KCl, 1.25 NaH_2PO_4, 10 D-glucose, 0.5 $CaCl_2$, 7 $MgCl_2$, 300-310 mOsm. Rodent brain slices were recovered in artificial cerebrospinal fluid (aCSF) identical to the recording solution. All experimental protocols were approved by the internal review board (IRB) and/or the institutional animal care and use committee (IACUC) at the respective institution(s).

Whole-cell patch clamp

All human and rat experiments were conducted under identical conditions. Slices were placed in a recording chamber and visualized with Dodt gradient contrast (Examiner Z1, Zeiss), while being perfused with the recording aCSF using a peristaltic pump (Minipuls, Gilson) at a flow rate of 1.6 mL/min, maintained at 36 °C with an inline heater (TC344B, Warner). The recording solution contained (in mM): 125 NaCl, 25 $NaHCO_3$, 3 KCl, 1.25 NaH_2PO_4, 10 D-glucose, 1.2 $CaCl_2$, 1.2 $MgCl_2$, 300-310 mOsm. All recordings were made from the soma of pyramidal neurons (PNs) in layer 2/3 (L2/3) of the human neocortex, or layer 5 (L5) of the rat temporal association area (TeA), using a MultiClamp 700B amplifier (Molecular Devices). Data were digitized and acquired with Prairie View (Bruker) at a sampling rate of 20 kHz, and subsequently analyzed with PVBS (https://github.com/flosfor/pvbs). Patch pipettes (2.5-4.5 MΩ) were pulled from borosilicate glass capillaries (PG52151-4, WPI) with a horizontal pipette puller (P-1000, Sutter), and positioned using micromanipulators (Junior, Luigs & Neumann). The internal solution contained (in mM): 130 K-gluconate, 4 KCl, 4 NaCl, 10 HEPES, 15 phosphocreatine-di(tris), 4 Mg-ATP, 0.3 Na2-GTP, adjusted to pH 7.3 with KOH (typically 6-8 mM of additional K^+ from KOH), 300-310 mOsm, with additional 0.05 mM Alexa Fluor 594 and 0.1 mM Oregon Green BAPTA-1 (Thermo Fisher) for visualization and calcium imaging. Pipette capacitance (C_p) was fully compensated, typically 13-

14 pF. Series resistance (R_s) was continuously monitored throughout the course of recordings, and cells with Rs ≤ 20 MΩ with less than 15% change were accepted. To measure the intrinsic neuronal membrane properties, cells were held in current clamp at 0 pA, and injected at the soma with current steps of 50 pA resolution (-250 pA to +1000 pA, 500 ms or 1000 ms duration), with bridge fully balanced. R_{in} was calculated from the linear fit crossing the origin obtained from the transient membrane potential responses to step current input in order to minimize the contribution from hyperpolarization-activated current (i_h). Sag ratio was defined as the difference between the transient and steady-state voltage response, divided by the transient voltage response in alignment with the definition of R_{in}. For the analysis of action potential (AP) waveforms, the first AP generated at rheobase was used. AP threshold was defined as the membrane potential immediately before the point at which dV/dt first exceeded 10 (V/s). AP amplitude was calculated as the difference between the AP peak and AP threshold, and the width at half of this amplitude was taken as AP half-width. Liquid junction potential was measured at 11-12 mV, but was not corrected for in the membrane potential values reported in the current study.

2-photon glutamate uncaging and calcium imaging

2-photon excitation microscopy (2PEF) for simultaneous structural imaging, glutamate uncaging (2PGU), and calcium imaging was performed using two Ti:sapphire lasers (Mai Tai eHPDS, Spectra Physics), modulated with four electro-optic modulators (M350-80, Conoptics) combined with custom optical elements including a 8x pulse splitter (https://flosfor.github.io/pulse_splitter.pdf). For structural and calcium imaging, cells were visualized with 0.05 mM Alexa Fluor 594 and 0.1 mM Oregon Green BAPTA-1 included in the internal solution as described above, respectively excited with 880 nm or 920 nm. Emission signals were acquired with two photomultiplier tubes (H7422-40, Hamamatsu). Optical elements in the excitation and emission pathways were obtained from Thorlabs or Chroma, unless otherwise specified. For calcium imaging, line scans (typically 256 repetitions of ~1 ms durations) were made across the dendritic branch near the center of the synaptic spines activated with 2PGU. The region of interest (ROI) and background for calcium imaging signals were defined respectively as those regions with signal intensities above the 2nd percentile or below the 50th percentile during the baseline period prior to 2PGU pulse delivery. For 2PGU, 5 mM MNI-caged-L-glutamate (Tocris) was dissolved in recording aCSF (adjusted to 120 mM NaCl to compensate for osmolarity), loaded and delivered with a puffer pipette of pore size ~15 to 20 um in diameter, positioned ~100 um away from the synaptic spines at a vertical angle of 20 degrees. Spines were activated with 720 nm excitation, quasi-simultaneously at an interval of 0.12 ms with a dual galvanometer scanner (Bruker), at an intensity producing physiological uEPSP amplitudes at the range of ~0.1 to 0.5 mV (typically corresponding to ~50 to 100 mW when measured with continuous full-field illumination, instead of short, focalized pulses used for actual 2PGU experiments), and ~0.1 um from the head of dendritic spine. 20 to 35 spines were activated at a given time, typically spanning 30 to 40 um along the dendritic branch.

Data analysis

Electrophysiology and calcium imaging data were analyzed and visualized using PVBS (https://github.com/flosfor/pvbs). Structural imaging data were processed with imageJ (https://imagej.net). Plots were made using custom codes written in MATLAB (Mathworks), and Prism (GraphPad). Statistical information is expressed as mean ± standard error of the mean (SEM), where n indicates the number of branches or cells, as applicable. The level of statistical significance was accepted when $P < 0.05$ (* $P < 0.05$; ** $P < 0.01$; *** $P < 0.001$) with Mann-Whitney U test, unless otherwise specified.

Acknowledgements

This work was supported by the Y. Eva Tan Postdoctoral Fellowship from the Yang-Tan Center for Molecular Therapeutics in Neuroscience at MIT.